PHYSICAL REVIEW A VOLUME 18, NUMBER 3 SEPTEMBER 1978

Motional-Stark-effect spectroscopy: $7\,^1S$-$9\,^1P$ energy separation and Zeeman tuning parameters for ^{4}He

M. Rosenbluh, R. Panock, and B. Lax
Francis Bitter National Magnet Laboratory and Department of Physics, Massachusetts Institute of Technology, Cambridge, Massachusetts 02139

Terry A. Miller*
Bell Laboratories, Murray Hill, New Jersey 07974
(Received 30 May 1978)

The $7\,^1S$-$9\,^1P$ energy separation of ^{4}He has been measured by the method of laser magnetic resonance in electron-beam-excited ^{4}He. The measurements have also provided Zeeman tuning coefficients for terms up to fourth order in the field B. Motional-Stark-effect (MSE)-dominated line shapes are observed at most fields. These line shapes are analyzed, and their Doppler-free portions used to obtain a value for the energy separation with a precision exceeding 1 ppm ($\Delta E_o = 980.7979 \pm 0.0002$ cm^{-1}). Arguments are presented that show the importance of the MSE in magnetically confined hot plasmas and in certain collapsed stars possessing high magnetic fields.

I. INTRODUCTION

In recent years, the precision spectroscopy of ^{4}He, employing methods far more precise than those of conventional optical and infrared spectroscopy, has become an active area of atomic physics.[1-4] The need for precise data on He, the second most abundant universal matter, is easily justified. In addition, the precision measurements provide the necessary data for testing approximate solutions to the atomic three-body problem.[5-8] Interest in the general physics of atomic Rydberg states has also been growing recently,[9] especially with the work on laser excitation of alkalis by several groups.[10,11]

In a previous paper[1] we presented a new technique, which relies on the motional Stark effect (MSE), present in magnetic fields, for obtaining sub-Doppler spectra of molecules (atoms) in high magnetic fields. The present paper has a threefold purpose, each of which is considered separately in Secs. III, IV, and V. In Sec. II we describe the experimental apparatus. In Sec. III we expand on the concepts discussed in Ref. 1 (henceforth to be referred to as I) and provide some physical insight into the line-shape analysis presented there. In Sec. IV the results of applying the line-shape analysis to the $7\,^1S$-$9\,^1P$ transition of ^{4}He are presented. Along with the precise zero-field energy separation of these states we report measurements of the Zeeman tuning parameters, up to fourth order in the field B. Finally, in Sec. V we point to the presence and applicability of the MSE line shape to plasma diagnostics in tokamaks and to the spectra of certain high magnetic-field white dwarfs. (Interestingly, a related effect has also been observed recently[12] in a solid.) In the remainder of this introduction we present a brief review of some of the relevant previous precision spectroscopic work on He.

A. Survey of He energy intervals

The energy intervals of He can be conveniently broken into several categories: (i) The relativistic fine-structure intervals involving a change of the J quantum number within a triplet state; (ii) the separation between the singlet and triplet terms of the same principal quantum number n and angular momentum quantum number L; (iii) electrostatic fine-structure intervals involving a change in L for a given n state; (iv) energy intervals where n and L change. There are also a few precision measurements concerning the different Zeeman parameters and g factors for the He atom.

Historically, the measurements of conventional optical spectroscopy were of type (iv).[13] More recently much higher-precision experiments have focused primarily on the other three categories. The microwave optical magnetic resonance experiments of Lamb and co-workers,[14] involving relativistic fine-structure intervals were the first to greatly improve on the previously available optical data. Similar measurements using the molecular-beam-microwave-resonance technique[15] have since led to some of the most precisely measured energy intervals in He. (For example, the $2\,^3P_0$-$2\,^3P_1$ interval has been measured to precision of ~1 ppm.[15]) These measurements have been the motivating force behind the extensive and precise calculations of Pekeris and co-workers,[6] whose calculated energies agree with experiments to

better than 10 ppm.

Level anticrossing experiments (for $n = 3$–9) of Miller and Freund[2] have resulted in a determination of the singlet-triplet separation for the D states. Beyer[4] has extended these measurements to even higher n (=20). The microwave-optical resonance experiments of MacAdam *et al.*[3] have yielded electrostatic and relativistic fine-structure intervals as well as some singlet-triplet separations. The electrostatic intervals for P-D (n = 16–18), D-F (n = 6–12) and F-G (n = 6) were measured. Singlet and triplet separations for the D, F, and G states were also measured for a number of different n values, along with numerous relativistic fine-structure intervals. The precision in some of the MacAdam measurements is of the order of 1 ppm.

All of these experiments have provided a valuable test for the Bruckner-Goldstone variational theory developed by Chang and Poe,[5] who have calculated singlet-triplet separations and electrostatic fine-structure intervals in terms of an inverse power series in n with only the odd powers greater than or equal to 3 contributing. Their predictions agree with experiment to about 1%. The polarization theories of Deutsch[7] predict electrostatic fine-structure intervals with a ~6% agreement with experiment.

The measurements reported in this work represent a return to the measurements of intervals of type (iv), but with techniques capable of much higher precision than the conventional optical techniques. We have measured[16] intervals such as $4\,^3S$-$4\,^3P$, $7\,^1S$-$9\,^1P$, $8\,^3S$-$12\,^3P$, etc. with better than 1-ppm accuracy and here we report on one of these intervals, the $7\,^1S$-$9\,^1P$ transition, for which our analysis is complete. We note that in comparison with other precisely measured intervals these transitions are unique in two respects. (a) They involve S and P states where the atom is most nonhydrogenic and thus provides the most severe test for the approximate three-body theories. (b) The transitions usually involve a change in the principal quantum number n. To our knowledge there are no theoretical calculations to predict such intervals, with the notable exception of the calculations of Schiff *et al.*[6] who calculate energies for S states up to $n = 15$ but for P states only to $n = 5$. Seaton's[17] empirical quantum-defect formalism, which is based on relatively low-precision optical data provides, surprisingly high-precision values for these intervals.

II. EXPERIMENT

Our experiments were performed using an infrared (CO_2) laser[18] to induce transitions between

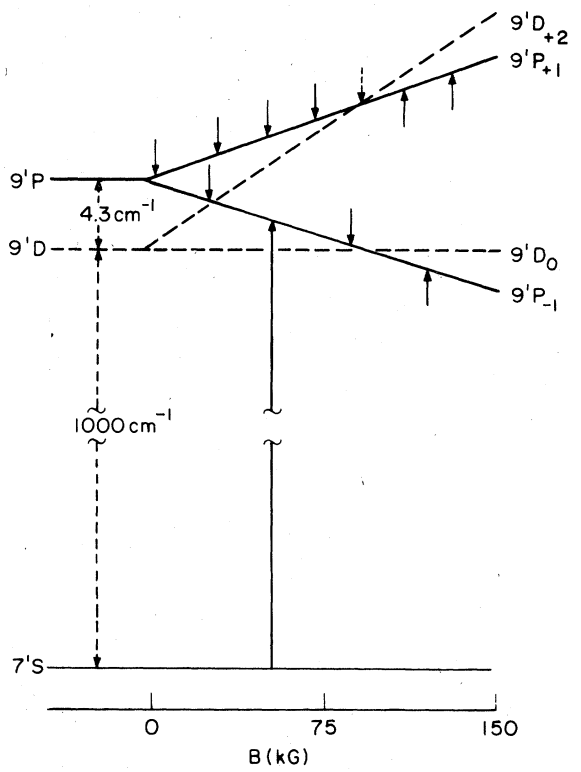

FIG. 1. Zeeman tuning curves for the He $7\,^1S$ and some $9\,^1P$ levels. Shown by arrows are the field positions where magnetic resonance line shapes were observed. The Zeeman tuning of some $9\,^1D$ levels is shown since it is important in the calculation of the polarizability.

different Zeeman sublevels of the electron-bombardment-excited He atom. The magnetic field provided the tunability (~13 cm^{-1}) needed to sweep through a resonance as well as allowing us to measure the Zeeman parameters. What is perhaps even more important, the magnetic field is the source of the motional Stark field seen by the atom in its rest frame and is thus the source of the unique MSE line shape to be discussed in Sec. III.

The experimental apparatus has already been briefly described in I. In Fig. 1, a schematic energy level diagram of the He $7\,^1S$ and two of the $9\,^1P$ levels is shown for magnetic fields ranging from 0 to 150 kG. Shown by arrows, along the $9\,^1P$ Zeeman sublevels, are the fields where the $7\,^1S$-$9\,^1P$ Zeeman sublevel separation frequency is equal to a CO_2 laser frequency. Resonance measurements were made at each of the indicated fields in Fig. 1, by preparing singly excited He atoms in the $7\,^1S$ state, using electron bombardment, and then driving the $7\,^1S$-$9\,^1P$ transition with a CO_2 laser

as the magnetic field was swept. The signal was detected by monitoring the emission from the 7^1S excited state to the 2^1P state at 4024 Å, as a function of magnetic field. For a few of the lines the 9^1P-2^1S emission was also monitored to yield a complementary signal.

The magnetic field was measured using a previously described NMR spectrometer[19] in conjunction with a temperature-stabilized Hall probe. The laser frequency was inferred to the desired accuracy from available measurements,[20] by keeping the laser tuned very close to the top (center) of the gain profile. The laser power was continuously monitored and when needed, the laser was returned to the gain center frequency. The gas pressure was measured on an MKS Baratron gauge and the excitation electron current was feedback stabilized to keep it constant.

The data were obtained by sweeping over a predetermined magnetic field range, a large number of times (10–60 with about 1 min per sweep) and additively averaging the signal in a Fabritek data averager. For analysis the data were transferred onto magnetic tape and to a PDP-11 computer, on which the line-shape fitting, described in Sec. IV, was performed.

Data was obtained at 10 out of 11 different positions along the Zeeman sublevels shown in Fig. 1. The reasons why no data was obtained for the 11th resonance (at ~92 kG on the $m_l = +1$ branch) will be given in Sec. IV. The three controllable parameters that could contribute to spectral line broadening, laser power, excitation electron current, and gas pressure were kept as low as possible so as to avoid line broadening by them. Measurements indicate that the $\lesssim$1-mA excitation current caused ~5-MHz halfwidth at half maximum, (HWHM) broadening, and that the 5–8 mW of laser power contributed ~6 MHz (HWHM). We were not able to see a noticeable pressure-broadening effect, however, a calculated estimate of pressure broadening for the $n = 9$ state of He is ~1 MHz/μm of pressure. The pressure in the excitation chamber for all the resonances was approximately 10 μm.

A number of other, uncontrollable, contributions to line broadening were present in our experiments, including the residual magnetic-field inhomogeneity and instabiltiy, the states natural lifetime and the gas temperature. The field inhomogeneity is a function of the magnet temperature and thus it is a function of field and the season of the year, since the coolant water temperature depends on the season. At about 20 kG the homogeneity is always better than ~±3 G over a 2-cm length of bore. At 140 kG the inhomogeneity ranges from ~8 G/cm (~11 MHz/cm) to ~20 G/cm (~28 MHz/cm) for winter and summer, respectively. The magnet is feedback stabilized to keep field fluctuations in time under ~±1.5 G (≈±2 MHz) for extended periods (hours). Helium atomic state lifetimes are available from calculations and the 9^1P lifetime (by far the shorter of the two) is reported to be ~44 nsec.[21] This lifetime implies a natural linewidth (HWHM) contribution of ~10 MHz. However, at the experimental pressures, some radiation trapping almost certainly occurred, lengthening this lifetime, and thus reducing the contribution.

At zero field the largest linewidth contribution, by far, would be from the Doppler effect. Since the 7^1S-9^1P resonances were all around CO_2 laser frequencies, the Doppler linewidth [$\Delta\nu = 2\nu_0(v_0/c)(\ln 2)^{1/2}$ at FWHM] for He at room temperature is ≈130 MHz. We were able to experimentally determine the gas temperature from the linewidth of the resonance at 2 kG, the only resonance where the MSE is negligibly small. (At 2 kG the MSE shifts the resonance frequency of a thermal velocity atom by less than 1 MHz.) The line shape obtained at this field was well fit by a Voigt profile, from which both the temperature- and velocity-independent linewidth were determined. The gas temperature was actually found to be ~450 °K. The actual temperature at a particular resonance (as determined from fitting the lines with the temperature-dependent MSE line shape, derived in Sec. III), however, varied from about 460 to 430 °K depending on the electron-gun temperature, magnet temperature, and gas pressure. The Voigt profile also indicated a ~17-G velocity-independent linewidth.

An independent measurement of the homogeneous linewidth was obtained from a Lamb dip, produced in the 2-kG resonance, when the laser beam was reflected back on itself through the interaction region. The origin of the dip can be understood, when one considers a transition which is nearly saturated by the incident driving laser. Since those atoms that have zero y velocity can interact with the laser beam twice (up and down) these atoms will already have been pumped to saturation. At some other $|\vec{v}_y|$, however, the laser can interact with the $-\vec{v}_y$ atoms in one direction and the $+\vec{v}_y$ atoms in the other direction so that these atoms would saturate at a slightly higher incident laser intensity than the $v_y = 0$ atoms.

The width of the dip is just the width of the residual velocity-independent component in the line (assumed to be all homogeneous contributions). The measurement of the Lamb-dip width also yielded a 17-G ≈ 23-MHz (FWHM) homogeneous contribution. Considering the size of the velocity-independent contributions outlined above this is a

most reasonable result. At higher fields the homogeneous widths were found (from the MSE line fitting) to be somewhat larger, probably due to the larger field inhomogeneity already discussed. For all other resonances studied the dominant line-shape contribution turned out to be due to the MSE, to which we now turn our attention.

III. MSE LINE SHAPE

A. Physical arguments

A derivation of the MSE line shape for the case where the homogeneous contribution is neglected is presented in I. It is also stated there that the line shape for the case where the homogeneous line shape is included can be obtained by convoluting the derived line shape with a Lorentzian. In the present discussion we would like to present a different derivation which includes the homogeneous contribution from the start, and arrives at results identical to those reported in I. First, however, we present some physical arguments that indicate the essential features of the MSE line shape.

We start by considering a normal Doppler-broadened line shape (a Gaussian), as shown in Fig. 2. Since the Doppler frequency shift and the atomic velocity parallel to the direction of observation are linearly related, $\Delta\nu = (v_y/c)\nu_0$, the horizontal axis in Fig. 2 can be interpreted as representing either v_y or $\Delta\nu$. (Here the laser propagates in the y direction, ν_0 is the absorption line center frequency, and $\Delta\nu$ is the frequency offset from line center due to the Doppler shift.) The vertical axis represents either the number of atoms with a given velocity v_y or the number of atoms absorbing light at a given frequency ν.

When an absorbing atom is in a region containing magnetic fields, another velocity-dependent frequency shift arises besides the normal Doppler shift. This frequency shift is due to the interaction of the atomic motion with the magnetic field. As the atom moves through the field with some velocity $\vec{v}$, in its own rest frame it sees not only the magnetic field $\vec{B}$, but also an electric field given by $\vec{F} = (1/c)(\vec{v}\times\vec{B})$. Since all atoms and molecules (including the hydrogen atom in a magnetic field) have zero permanent dipole moments, perpendicular to the magnetic field,[22] the atom or molecule will respond to the "motional electric field" in second order only. The frequency shift of a transition by the MSE will therefore be given by

$$\Delta\nu = (\alpha/hc^2)(v_x^2 + v_y^2)B^2 , \tag{1}$$

where we have assumed that $\vec{B}$ is along the z direction and α is one-half of the difference in polarizability of the states involved in the transition.

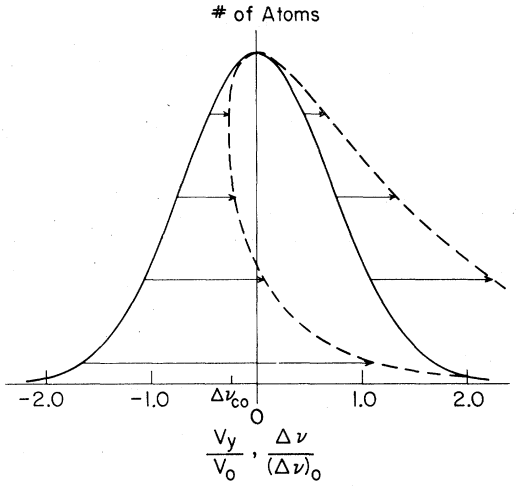

FIG. 2. Gaussian distribution showing the strength and direction of the motional Stark effect as a function of velocity.

Although the MSE is a two-dimensional problem, that is, the frequency shift depends on the motion of the atom in the plane perpendicular to the magnetic field, several aspects of the resultant line shape can be inferred by considering motion only in the direction of the propogation of the light. Thus we set v_x equal to zero and consider the minimum motional Stark shift experienced by an atom with a given v_y. The arrows in Fig. 2 indicate the frequency to which a group of atoms with velocity v_y are shifted due to this effect. The dashed curve is drawn to indicate the frequency at which an arbitrary velocity group will absorb (emit). We can then immediately see from Fig. 2 that there must be a frequency cutoff $\Delta\nu_{\text{cutoff}}$, that is, a frequency below which no atoms can absorb light. If we were to allow each atom to have some velocity in the x direction this would not change the position of the cutoff since any atom with $v_x \neq 0$ would absorb at even higher frequencies than the cutoff frequency.

Mathematically one can write the net frequency shift (with $v_x = 0$) as

$$f(v_y) = (\nu_0/c)v_y + (\alpha/hc^2)B^2 v_y^2 . \tag{2}$$

Finding the minimum of $f(v_y)$ is equivalent to finding the minimum of the dashed curve in Fig. 2. Thus we find the cutoff velocity, that is, the value of v_y for which $f(v_y)$ is a minimum is given by

$$v_y^{\text{cutoff}} = -c\nu_0 h/2\alpha B^2 \tag{3}$$

and the frequency shift at that point is

$$\Delta\nu_{\text{cutoff}} = f(v_y^{\text{cutoff}}) = -\nu_0^2 h/4\alpha B^2 \equiv \nu_0 - \nu_{\text{cutoff}} \tag{4}$$

which is identical to that given in I.[23]

A number of significant observations can be made on the basis of Eq. (4) and Fig. 2. First we note that at the cutoff frequency ν_{cutoff} we can expect an abrupt, discontinuous rise in the line shape. This is due to the fact that there are a finite number of atoms with the cutoff velocity, v_y^{cutoff} and $v_x = 0$, and all of these atoms will contribute at the cutoff frequency. Second, we point out that at this sharp, discontinuous cutoff only those atoms with $v_x = 0$ can contribute since all atoms with $|\vec{v}_x| > 0$ will have a MS shift that is greater than the shift for $v_x = 0$. Third, we can see that the cutoff frequency will be either above or below line center (ν_0), depending only on the sign of α, and it approaches ν_0 rapidly as αB^2 gets large. Since even for moderate values of αB^2 the cutoff occurs very close to line center ν_0, the line shape is called sub-Doppler. As a last point it is interesting to note that the cutoff frequency is temperature independent. That is, it occurs at the same distance from line center in frequency space, independent of the width of the Doppler curve with which one starts.

Based on Fig. 2, and the arguments just presented we cannot say what the line shape will look like beyond the cutoff frequency. It is, however, clear that for large enough values of α the line shape will decay at a slower rate than the original Doppler profile. This occurs because the fast moving atoms get shifted much farther from the center frequency ν_0 by the MSE since the frequency shift goes as the square of the velocity. Also, the absorption or emission of a single velocity group whose width in frequency space was only the homogeneous width has now been drastically broadened due to the motion in the x direction. As we shall see, this expectation is correct, and the line decays as a slow exponential with an exponent proportional to $(v_0^2\alpha B^2/c^2)^{-1}$, where v_0 is the thermal velocity ($v_0^2 = 2kT/M$) and T is the temperature.

The inclusion of a homogeneous contribution in the line-shape analysis does not significantly alter the line shape as long as the homogeneous width is small ($\Delta\nu_H < \Delta\nu_D < \Delta\nu_{\text{MSE}}$). In fact, as we will show, the homogeneous contribution shows its effect most notably on the sharp cutoff, which acquires a finite slope proportional to the homogeneous width.

B. Line-shape derivation

Let us now proceed to derive the spectroscopic line shape of a thermal distribution of atoms in the presence of a homogeneous magnetic field. The three mechanisms that will contribute to the line shape are the homogeneous contribution, the Doppler shift, and the MSE. We start by writing the characteristic response of an atom (a damped resonant system) as

$$g_H(\nu) = \Delta\nu_H/2\pi[(\nu - \nu_0)^2 + (\Delta\nu_H/2)^2] \tag{5}$$

which is the well-known Lorentzian line-shape function with $\Delta\nu_H$ the homogeneous linewidth (FWHM). To obtain the line shape in the presence of the Doppler effect and MSE we substitute for $\nu - \nu_0$ ($\equiv\Delta\nu$) in Eq. (5), the velocity-dependent resonance condition,

$$\Delta\nu - [v_y\nu_0/c + \alpha B^2(v_x^2 + v_y^2)/hc^2] = 0$$

and integrate the result over a Maxwell-Boltzman distribution of velocities. (This procedure is identical to the method used in obtaining the Voigt profile, which is a combination of homogeneous and Doppler contributions). Thus we obtain

$$g(\nu) = \frac{1}{2\pi^{5/2}v_0^3}\int\int\int_{-\infty}^{\infty} \frac{\Delta\nu_H \exp\{-[(v_x^2 + v_y^2 + v_z)/v_0^2]\}\, dv_x\, dv_y\, dv_z}{\{\nu - \nu_0(1 + v_y/c) - \alpha B^2(v_x^2 + v_y^2)/hc^2\}^2 + (\Delta\nu_H/2)^2}\ . \tag{6}$$

The v_z integration can be easily performed to yield a factor of $(\pi^{1/2}v_0)$. Let us now translate coordinates to u and v and define a number of quantities which will help in simplifying Eq. (6). Thus

$$\begin{aligned}
&u \equiv v_y/v_0 + hc\nu_0/2v_0\alpha B^2\,,\\
&v \equiv v_x/v_0\,,\\
&a^2 \equiv (hc^2/\alpha B^2)(\Delta\nu + h\nu_0^2/4\alpha B^2)\,,\\
&\gamma_D \equiv h\nu_0 c/\alpha B^2 v_0\,,\\
&\gamma_H \equiv h\Delta\nu_H c^2/\alpha B^2 v_0^2\,,\\
&\gamma \equiv hc^2\Delta\nu/\alpha B^2 v_0^2\,,
\end{aligned} \tag{7}$$

and

$$b^2 \equiv \ + \tfrac{1}{4}\gamma_D^2\,.$$

[The γ's just defined possess physical significance; γ_D is the ratio of the Doppler shift to the MS shift for an atom with speed v_0 while γ_H is the ratio of the homogeneous width (FWHM) to the MS shift for a v_0 atom; γ is the frequency offset from line

center in units of the MS shift for a v_0 atom.] Using these definitions we can rewrite Eq. (6) as

$$g(\Delta\nu) = (\gamma_H hc^2/2\pi^2 v_0^2 \alpha B^2)\exp(-\gamma_D^2/4) \times \int_{-\infty}^{\infty} du \exp[-(u^2 - \gamma_D u)] \times \int_{-\infty}^{\infty} \frac{dv \exp(-v^2)}{(b^2 - u^2 - v^2)^2 + \gamma_H^2/4} . \quad (8)$$

If we now change from rectangular to polar coordinates, one of the integrals can be manipulated into the form of a modified Bessel function $I_0(\beta)$. Therefore letting

$$u \equiv r\sin\theta, \quad v \equiv r\cos\theta, \quad u^2 + v^2 = r^2$$

and

$$du\, dv = r\, dr\, d\theta$$

we obtain

$$g(\Delta\nu) = (\gamma_H hc^2/2\pi^2 v_0^2 \alpha B^2)\exp(-\gamma_D^2/4) \times \int_0^{\infty} dr \frac{r\exp(-r^2)}{(b^2 - r^2)^2 + \gamma_H^2/4} \times \int_0^{2\pi} d\theta \exp(\gamma_D r\sin\theta) . \quad (9)$$

The θ integral is a modified Bessel function of order zero

$$I_0(\beta) \equiv \frac{1}{2\pi}\int_0^{2\pi} d\theta \exp(\beta\sin\theta)$$

so we can rewrite Eq. (9) as

$$g(\Delta\nu) = (\gamma_H hc^2/\pi v_0^2 \alpha B^2)\exp(-\gamma_D^2/4) \times \int_0^{\infty} dr \frac{r\exp(-r^2) I_0(\gamma_D r)}{(b^2 - r^2)^2 + (\gamma_H/2)^2} . \quad (10)$$

A final simplification of Eq. (10) can be obtained by defining

$$x \equiv r^2, \quad x_0 \equiv b^2, \quad y \equiv x - x_0 ,$$

and therefore

$$dx = 2r\, dr, \quad dy = dx .$$

This results in

$$g(\Delta\nu) = (\gamma_H hc^2/2\pi v_0^2 \alpha B^2)\exp[-(\gamma_D^2/2 + \gamma)] \times \int_{-x_0}^{\infty} dy \frac{I_0(\gamma_D (y + x_0)^{1/2})\exp(-y)}{y^2 + (\gamma_H/2)^2} \quad (11)$$

which is our final result for the MSE line shape.

An examination of the integral in Eq. (11) shows that it is really an integral over a product of three functions; $I_0(\beta)$, an exponential, and a Lorentzian. For the case where the Lorentzian is a sharp function [compared to $I_0(\beta)$ and the exponential, i.e., just about all physically real situations] the integral will be finite only when the integration includes the region of y space where the Lorentzian lies. Since the Lorentzian is always peaked at $y = 0$, the integral will be zero if $-x_0 > 0$, it will vary as $-x_0$ goes through zero, and becomes a constant for $-x_0 < 0$. Under the assumption that the Lorentzian width is narrow and neither $I_0(\beta)$ or the exponential vary much over the Lorentzian width, they can be pulled out of the integral. Then the integral reduces to

$$\int_{-x_0}^{\infty} (y^2 + \gamma_H^2/4)^{-1} dy = (4/\gamma_H^2)[\tan^{-1}(4\chi_0/\gamma_H^2) + \tfrac{1}{2}\pi]$$

which is identical to Eq. (6), given in I, and is the source of the sloping cutoff. Since the integral contributes to the line shape only over the region where the Lorentzian lies, for other values of $\Delta\nu$, the integral is just a numerical constant, and the line shape is dominated by the exponential outside the integral, which is the source of the long exponential tails. It can be shown, that in the limit of no MSE, Eq. (11) reduces to a Voigt profile.

If the spectral line is not swept out in frequency space (for lack of tunable laser, for example) but rather by Zeeman tuning the resonance over a fixed (laser) frequency, Eq. (11) needs to be trivially modified to obtain the line shape $g(\Delta B)$. (The experiments in which these line shapes were observed are actually field swept.) The modification consists of replacing $\Delta\nu$ in Eq. (11) by

$$\Delta\nu = \mu_0 g_e (B - B_0) = \mu_0 g_e \Delta B , \quad (12)$$

where μ_0 is the Bohr magneton and g_e is an effective g factor as determined by the linear Zeeman effect for the levels involved in the resonance.

IV. MEASUREMENT OF THE 7^1S-9^1P TRANSITION

A. MSE line-shape-fitting parameters

In order to determine the size of the MSE we must obtain a value for α, the effective polarizability for the states involved in the transition. To do this we use hydrogenic wave functions and calculate the matrix elements $\langle\Psi_1 | x | \Psi_2\rangle$. We find that the Stark-shifted energy for a state with quantum numbers (n, l, m_l) is given by

$$E^{(2)}_{n,l,m} = \left(\frac{3nea_0}{4}\right)^2 \left[\frac{n^2-(l+1)^2}{(2l+3)(2l+1)} \left(\frac{(l+m+1)(l+m+2)}{E_{n,l,m} - E_{n,l+1,m+1}} + \frac{(l-m+1)(l-m+2)}{E_{n,l,m} - E_{n,l+1,m-1}} \right) \right.$$
$$\left. + \frac{n^2-l^2}{(2l+1)(2l-1)} \left(\frac{(l-m)(l-m-1)}{E_{n,l,m} - E_{n,l-1,m+1}} + \frac{(l+m)(l+m-1)}{E_{n,l,m} - E_{n,l-1,m-1}} \right) \right] F^2$$
$$\equiv -\tfrac{1}{2}\alpha' F^2 . \qquad (13)$$

We use Eq. (13) as the definition of the polarizability α', and define 2α to be the difference in polarizability of the states involved in the transition,

$$2\alpha \equiv -\alpha'(\text{upper state}) + \alpha'(\text{lower state}). \qquad (14)$$

In writing Eq. (13) we have assumed that only states with the same quantum number n give a significant contribution to α'. This is a very reasonable approximation for the $n=9$ states, since the energies of the $n=10$ terms are far removed. The hydrogenic approximation used in obtaining Eq. (13) can also be shown to be very good. (If one extrapolates the Bates-Damgaard coefficients[24] to $n_l^* = 9.002$, and uses $n_{l-1}^* - n_l^* = -0.014$, one finds that the correction to the hydrogenic matrix elements is much less than 1% of the hydrogenic values.) Also, the energy differences appearing in Eq. (13) are generally known with an accuracy exceeding a few percent from conventional spectroscopic and more recent precision measurements.[13] Thus α' can be reliably calculated with a precision exceeding 2%–3%, which is sufficient for accurately fitting the observed spectral line shapes. Recently, we have also been able to test the accuracy of our polarizability calculations with a direct experiment. This was accomplished by placing Stark plates inside the excitation chamber (electric field along $\pm x$ direction) and measuring the shift of the 7^1S-9^1P resonance (at ~2 kG) as a function of applied electric field. The calculations agreed with experiment to ~5%, which was also the experimental uncertainty in the measurements.

Because the energy denominator in Eq. (13) is field dependent α' cannot be assumed to be a constant in a magnetic resonance experiment. Thus the MSE will generally grow due to the B^2 dependence of the motional electric field and it will also grow or diminish due to the Zeeman tuning of the interacting levels.[25] The Zeeman tuning contribution becomes particularly important near anticrossings of the interacting levels. Two such anticrossings occurred in the 9^1P state between the $9^1P_{+1} - 9^1D_{+2}$ and $9^1P_{-1} - 9^1D_0$ sublevels as indicated in Fig. 1. Calculated values for $(\alpha' v_0^2/2c^2)B_0^2$, the shift (in kG) of the resonance field of a thermal velocity atom, due to MSE, are listed in Table I for the eleven transitions indicated in Fig. 1. The effect of the anticrossings on α' are clearly large. The Table also lists the ratios of the MSE shift to the Doppler frequency shift for a v_0 (thermal velocity) atom, using the cal-

TABLE I. Calculated values of the shift (in kG) of the resonance field of a thermal velocity v_0 ($T \simeq 400$ °K) atom, from the line center (B_0) due to the MSE. Also listed are the ratios of the MSE shift to Doppler shift for a v_0 atom ($\nu_0 \simeq 3\times10^{13}$ Hz). The magnetic fields B_0 used in the calculation corresponds to the observed (except at 91.5 kG) resonance fields. Equations (1) and (13) were used in the calculation with values for the energy denominators in Eq. (13) taken from Martin.[13]

B_0 (kG)	$\Delta\nu'_{MS}$ (9^1P) (kG)	$\Delta\nu'_{MS}$ (7^1S) (kG)	$\Delta\nu_{MS}$ (kG)	|MSE/Doppler|
118.428	−0.173	−0.016	−0.157	1.7
83.810	0.569	−0.008	0.577	6.3
52.564	0.129	−0.003	0.132	1.4
23.974	0.027	<−0.001	0.027	0.3
2.468	<0.001	<−0.001	<0.001	0.0
27.068	0.051	<−0.001	0.051	0.6
50.071	0.256	−0.003	0.259	2.8
71.663	1.059	−0.006	1.065	11.6
91.500	≤−77	−0.010	≤−77	>800
111.152	−2.302	−0.014	−2.288	24.9
129.238	−1.593	−0.019	−1.574	17.2

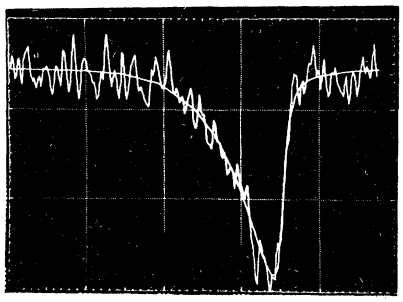

FIG. 3. Observed and calculated magnetic resonance line shape with a B_0 of 27.068 kG (on the $m_l=+1$ branch of the $9\,^1P$ state). The averaging time for obtaining the line shape was 7 min, with 5 mW/cm^2 of $R30$(10-μm branch) laser power. The excitation electron current was 1 mA and the gas pressure was 15 μm. The calculated line shape assumed a temperature of 440°K, a velocity-independent homogeneous width of 25 G and a motional Stark shift for a v_0 atom of 56 G.

TABLE II. Parameters used in fitting the observed line shapes. The quantity $\Delta\nu_{MS}$ is the shift of the resonance field of a thermal velocity (v_0) atom, due to the MSE. It is calculated from Eq. (1) and contains both the temperature T and the parameter α (one-half of the effective polarizability of the transmission).

Laser line (10-μm branch)	B_0 (kG)	$\Delta\nu_H$ (kG)	T (°K)	$\Delta\nu_{MS}$ (kG)
$R20$	118.428 ± 5	0.028	470	>-0.262
$R22$	83.810 ± 15	0.020	435	0.627
$R24$	52.564 ± 5	0.018	445	0.147
$R26$	23.974^{+5}_{-10}	0.018	460	0.031
$R28$	2.468 ± 2	0.017	450	0
$R30$	27.068 ± 4	0.025	440	0.056
$R32$	50.071 ± 4	0.024	440	0.285
$R34$	71.663^{+9}_{-3}	0.026	435	1.158
$R36$	Complicated spectrum; not analyzed.			
$R38$	111.152^{+5}_{-8}	0.030	430	-2.459
$R40$	129.238 ± 4	0.010	454	-1.786

culated α's and typical temperatures and frequencies ($T\approx 400$°K, $\nu_0\simeq 3\times 10^{13}$ Hz).

An experimentally obtained resonance at 27 kG on the $m_l=+1$ branch of the $9\,^1P$ state is shown in Fig. 3. Also shown in the figure is a theoretical fit based on Eq. (11) of the previous section. Considering that the laser power, gas pressure, and excitation electron current were all minimized, the signal to noise in this resonance (averaging time ~7 min) is very good. Unfortunately the signal to noise is not so good for all the resonances. This is due to the very broad lines that one obtains when working in a region of high αB^2. Since the total number of atoms participating in the resonance remains the same, the integrated intensity in the line must also remain constant. Thus for very large α, this leads to such a large line broadening that eventually the signal completely disappears for practical purposes.

When fitting a line such as shown in Fig. 3 one needs to specify as many of the four free parameters in Eq. (11) ($\alpha, B_0, T, \Delta\nu_H$) as possible. In our He experiments we were interested in obtaining accurate values for the field position of the center of the resonance B_0, and thus to obtain the best possible values we needed to fix the effective polarizability α, the gas temperature, and the width of the velocity-independent component of the line shape which we always assumed to be Lorentzian.

As already discussed, the polarizability α is calculable from Eq. (13) to a sufficient accuracy. The other two parameters, however, the temperature and velocity-independent width could only be constrained to lie within a fairly narrow range as determined from the low-field Voigt profile and Lamb-dip measurements. The fact that we could not accurately specify the temperature did not effect the determination of B_0, however, since the cutoff field (frequency) is temperature independent. In fact, the temperature most seriously affects the exponential tail, and thus can be determined from fitting the tail. Similarly the homogeneous width does not significantly affect the value of the cutoff field or for that matter the line shape as long as the MSE is large. Its effect shows up as a slope at the cutoff portion of the line and can be determined by fitting the slope.

In Table II we list the fitting parameters for all the observed resonances, along with the values of B_0 obtained from the fitting. The indicated errors for B_0 are an estimated sum of the effects of measurement and fitting uncertainties. With the exception of the 118.428-kG resonance, the values of α used to fit the observed line shapes are the same as the calculated values listed in Table I. [The actual quantities ($\alpha v_0^2 B_0^2/c^2$) appear to be different in the two tables since the temperature used in Table I was assumed to be 400°K for all the resonances.] The line-shape fitting was performed by assuming a calculated α, and varying T and $\Delta\nu_H$ until a good fit was obtained. Once a "correct fit" was found, all the parameters (including α) were varied to see how much effect they have on the goodness of the fit and on B_0, the field at line center obtained from the fit. In all the observed line shapes, only one set of values for the four parameters ($B_0, \alpha, T, \Delta\nu_H$) were found to give a "good" fit. In the ~118-kG resonance no reasonable combination of α and T provided a good

fit. However, even in this resonance a cutoff was well defined and B_0 could be easily obtained with a fair amount of confidence. For all the other resonances the experimental and theoretical line shapes showed good agreement.

As mentioned before we did not obtain any data for the 92-kG resonance on the $m_l = +1$ Zeeman sublevel. When we looked for this resonance a rich and complicated spectrum (with features over more than a 5-kG range) was observed which has not as yet been fully interpreted. We believe that the complexity of this resonance is due to two related factors. Since the resonance would occur very close to a 9^1P-9^1D anticrossing, α is very large and the signal would tend to wash out (for the reasons outlined above). What is more, near an anticrossing the levels do not tune even approximately linearly with field, thus contributing a complicated nonlinear broadening component to the line shape.

B. Zero-field separation and Zeeman parameters of the 7^1S-9^1P He levels

In order to obtain zero-field separations from the magnetic resonance data one must be able to specify the Zeeman tuning coefficients involved in the transition. In general the Zeeman tuning of a particular level can be represented by a Hamiltonian of the form

$$H_Z = \mu_0 g_s(\vec{B}\cdot\vec{S}) + \mu_0 g_L(\vec{B}\cdot\vec{L}) + H_{QZ}, \tag{15}$$

where H_{QZ} is the diamagnetic (quadratic) term. The first two terms in Eq. (15) merely represent the linear Zeeman effect. For those situations where the linear Zeeman eigenvalues can be evaluated in the decoupled term formalism (complete Paschen-Back effect) we obtain

$$E_{LZ} = \mu_0 B(g_s' m_s + g_L' m_L), \tag{16}$$

where we have used primes to indicate effective g values which include some well-known relativistic corrections.[26]

The quadratic contribution has been previously evaluated[27] to yield

$$H_{QZ} = (e^2/2mc^2)|\vec{A}(\vec{r})|^2, \tag{17}$$

where $\vec{A}(\vec{r})$ is the vector potential ($\vec{A} = \frac{1}{2}\vec{B}\times\vec{r}$) in the Coulomb gauge. Equation (17) reduces to

$$E_{QZ} = (e^2/8mc^2)B^2\langle r^2\sin^2\theta\rangle \tag{18}$$

which can be easily evaluated using hydrogenic wave functions to yield

$$E_{QZ} = \frac{e^2B^2}{4m^2c^2}\frac{l^2+l+m_l^2-1}{(2l-1)(2l+3)} \times \tfrac{1}{2}n^2[5n^2+1-3l(l+1)]. \tag{19}$$

The use of hydrogenic wave functions in Eq. (18) can be shown to be justifiable[28] if one substitutes $n^* = n - \delta$ for all the n's occurring in Eq. (19), where δ is the angular-momentum-dependent quantum defect.[17] There also exist terms that are proportional to B^4 and higher-order terms in the field B, which can be calculated, by taking into account the off-diagonal terms in the diamagnetic Zeeman Hamiltonian[27] H_{QZ} with the selection rules that only states with $\Delta l = \pm 2, 0$ and $\Delta m_l = 0$ are coupled.

The zero-field energy separation between the two levels involved in the transition can now be written as

$$\Delta E_0 = h\nu_{\text{laser}} + \Delta E_Z, \tag{20}$$

where $\Delta E_Z = \Delta E_{LZ} + \Delta E_{QZ} + \Delta E_{HZ}$ is the total Zeeman energy difference between the two levels. For the 7^1S-9^1P transition $m_s = 0$ for both levels and Δm_l in the transition is ± 1. Thus in Eq. (16) there is no relative Zeeman shift due to m_s and we obtain

$$\Delta E_{LZ} = \mu_0 B g_L', \tag{21}$$

where $g' = 0.99986 = 1 - m/M$ (all the other relativistic corrections to g' are much smaller and are neglected) and we can use the currently accepted value of $\mu_0 = 4.66860\times10^{-5}$ cm$^{-1}/G$.[29] The difference between the quadratic terms of the $7^1S(m_l = 0)$ and $9^1P(m_l = \pm 1)$ states can be evaluated using Eq. (19). If we use $\delta = +0.14$ for the ^1S state and $\delta = -0.012$ for the ^1P, in the quantum defect corrections ($n^* = n - \delta$), we obtain

$$\Delta E_{QZ} = (6.46984 - 1.84054)\times10^{-11}B^2 \ (\text{cm}^{-1}), \tag{22}$$

where B is measured in gauss.

We have used Eq. (20) to fit the 10 measured magnetic fields at the known laser frequencies[20] to a Zeeman tuning curve and have obtained empirical values for the quadratic and fourth-order coefficients as well as the zero-field separation of the 7^1S-9^1P transition. The fitting was performed, using a general polynomial least-squares fitting program on a PDP-11 computer.

In Table III we list the empirical zero-field energy interval and Zeeman tuning parameters, as well as earlier experimental and theoretical values for these quantities. The errors indicated with the measurements are for one standard deviation. It was gratifying that when the linear coefficient was allowed to be a variable in the fit we obtained a value for it (also listed in Table III) which is very close to the presently accepted physical constant.[29] The other coefficients and the zero-field energy did not change significantly when we allowed the linear coefficient to float.

In an attempt to obtain calculated values for the

TABLE III. Zero-field energies and Zeeman parameters for the $7\,^1S - 9\,^1P$ interval. The numbers in the first row of this table were obtained from a polynomial fitting program using the values of B_0 listed in Table II, and fixing the linear coefficient to be μ_0. The numbers in the second row are for the linear coefficient fixed at $g'\mu_0$ while in the third row all the coefficients including the linear Zeeman coefficient were obtained from the fit.

ΔE_0 (cm^{-1})	Linear Zeeman (cm^{-1}/G)	Quadratic Zeeman (cm^{-1}/G^2)	Fourth-order Zeeman (cm^{-1}/G^4)
980.7978 ± 0.0002	$[4.668\,60 \times 10^{-5}]$– fixed μ_B	$(4.645 \pm 0.009) \times 10^{-11}$	$(4.8 \pm 0.5) \times 10^{-23}$
980.7979 ± 0.0002	$[4.667\,95 \times 10^{-5}]$– fixed $g'\mu_B$	$(4.639 \pm 0.009) \times 10^{-11}$	$(5.3 \pm 0.5) \times 10^{-23}$
980.7978 ± 0.0002	$(4.668\,27 \pm 0.000\,13) \times 10^{-5}$	$(4.642 \pm 0.007) \times 10^{-11}$	$(5.0 \pm 0.4) \times 10^{-23}$
980.75 (From Ref. 13)			
980.7987 (Based upon quantum-defect theory[17])		(4.629×10^{-11}) Calculated from Eq. (22)	

higher-order terms included in ΔE_{HZ}, we have diagonalized the matrix of $\langle H_Z \rangle$, using as a basis the set of states for which $m_l = +1$ and $L = 1 - 8$, for fields ranging from 0 to 140 kG. As before the calculations made use of the hydrogenic approximation. The energy eigenvalues for the $9\,^1P$ state obtained from the diagonalization, were fit to a polynomial in B. We found that the series converges quite slowly and all even power terms up to 10 are required for a good fit.

The residuals (defined as the field calculated using the coefficients listed in Table III, minus the experimentally observed field) for the data points used in fitting the Zeeman tuning curve of the $9\,^1P$ state, are shown in Fig. 4 as a function of magnetic field. The fit was not significantly affected if any one of the ten data points was left out, and as can be seen the scatter does not seem to be systematic. The fitting procedure definitely indicated the need for terms of even order greater than 2. The data, however, did not allow us to distinguish between different higher-order terms. A best fit was obtained by allowing a B^4 term to exist and the coefficients for this term are listed in Table III. The calculated coefficient for the fourth-order term, which was obtained from the diagonalization described above, is ~25% higher than the experimental coefficient. However, if in the fitting of the calculated eigenvalues we only allowed terms up to fourth order, the calculations yielded a fourth-order coefficient within a few percent of the empirically obtained one. The best values for the empirically obtained energy and Zeeman parameters are $\Delta E_0 = 980.7979 \pm 0.0002$ cm^{-1}, quadratic coefficient $= (4.640 \pm 0.009) \times 10^{-11}$ cm^{-1}/G^2, and fourth-order coefficient $= (5.1 \pm 0.5) \times 10^{-23}$ cm^{-1}/G^4.

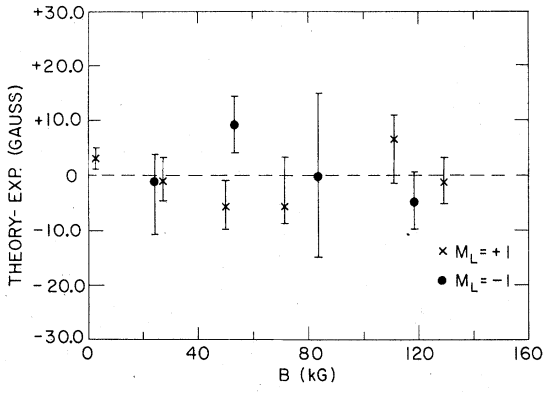

FIG. 4. Residuals (theory minus experiment) obtained from fitting the observed magnetic resonance line-center positions to a Zeeman tuning curve. The zero-field energy and Zeeman tuning coefficients used in the theory were those listed in third row of Table III.

Finally, we point to the great improvement in the value of ΔE_0 over the previously measured optical value.[13] As we have already pointed out the relative precision of our experiments is high because the energy intervals measured are large (~1000 cm^{-1} corresponding to CO_2 laser frequencies). Thus a small relative uncertainty in the tuning magnetic field is a much smaller relative uncertainty in the total transition frequency being measured. The fact that ΔE_0, as determined from Seaton's quantum-defect theory,[17] gives an interval that is much better than the previous spectroscopic value is rather surprising. The general accuracy of using Seaton's quantum defect theory in energy interval calculations has been previously noted.[3] The agreement between the calculated and measured quadratic coefficients is also surprisingly good. A new value for the quantum defects δ for the ^1S and ^1P states must await a number of other precision measurements of n^1S-n^1P intervals now under way.

V. MSE IN HOT PLASMAS AND STARS

For the MSE to be a large or the dominant line broadening effect one requires large magnetic

fields and high temperatures. Since the MSE linewidth is proportional to T (rather than $T^{1/2}$ as it is for the Doppler width) at any given magnetic field it eventually becomes the dominant effect as T is increased. Two natural places, other than our experimental apparatus, immediately suggest themselves as possible candidates for large (and indeed dominant) MSE broadening: magnetically confined hot plasmas (tokamaks) and collapsed stars that have trapped their small initial fields in their collapse (white dwarfs and neutron stars).

In this section we will briefly point to the reasons why we believe this previously ignored effect is dominant in some of these cases. The emphasis in these applications shifts from the Doppler-free portion of the line to the broad exponential tail. Another important difference between the considerations presented in this section and the He experiments is that here we are concerned with optical-uv emissions rather than infrared absorptions, but due to the high temperatures in the case of stars and plasmas the MSE dominates the Doppler effect even at these short wavelengths. Where possible we present some very rough order of magnitude calculations for these two examples.

A. Magnetically confined plasmas

Since we are most familiar with Alcator, the MIT tokamak, we shall refer to it specifically even though the same arguments apply to any other high-field tokamak. Alcator operates at a magnetic field of ~70± 10 kG. Since our previous experiments and calculations involved the polarizability α' of the $9^1P(m_l=+1)$ state of He we will consider it as a specific example. For higher-lying states of He the MSE becomes even more prominent while for lower ($n<5$) lying states it quickly disappears. (It is a negligible effect for transitions from states with $n\leq 4$). In view of the n^7 dependence in α', this is not surprising. A line width of $\sim 2\times 10^{11}$ Hz is calculated for the He 2^1S-9^1P emission from Alcator. The parameters used in this calculation are listed in Table IV. The estimated 5-eV temperature is a reasonable value for neutral atom temperatures near the wall of Alcator A.[30] We find, as shown in Table IV, that the MSE is about ten times bigger in this case than the Doppler effect. (In calculating the linewidth of the asymmetric line we have merely set the linewidth equal to the MSE shift of a v_0 atom.)

A few comments about the results listed in Table IV are in order. First, we emphasize that the ratio of linewidth to transition frequency is very large and easily resolvable with a standard dispersive element. Second, we point out that since the linewidth is proportional to temperature rather than the square root of temperature it provides a much more sensitive temperature probe than one would get from a normal Doppler profile. Lastly, whether one intends to measure the temperature from it or not, it should be kept in mind that the linewidth of neutral Rydberg state emissions from a plasma can be very wide, and the width often attributable to the MSE.

TABLE IV. Estimated MSE parameters for Alcator.

Transition: 2^1S-9^1P in He
Wavelength: 3258 Å $= 9.2\times 10^{14}$ Hz
Neutral temperature at wall: 5 eV $\simeq$ 58 000 °K
Doppler width of line at zero field: $=2\times 10^{10}$ Hz
Doppler width/transition frequency: =2 parts in 10^5
Magnetic field: $\simeq$ 70 kG
Motional stark shift of a v_0 atom at $T\simeq 400$ °K (see Table I): $\sim 1.4\times 10^9$ Hz $\approx$ 1 kG
Motional Stark shift of a v_0 atom at $T\simeq 5.8\times 10^4$ °K: $=2\times 10^{11}$ Hz
Linewidth of asymmetric line: $=2\times 10^{11}$ Hz
Asymmetric width/transition frequency: =2 parts in 10^4

There is a fair amount of evidence[31] that the neutrals inside the hot plasma come to thermal equilibrium with the ions very rapidly through the process of electron-exchange collisions. Thus, if one were to measure the temperature of such neutrals one could use it to determine the ion temperature. Actually there are two places in a tokamak where one would expect to find a substantial number of neutral atoms: (i) close to the wall, where the temperature is somewhat lower, and (ii) near the region where an energetic neutral beam of atoms is injected in order to heat the plasma. Thus, a neutral-temperature measurement obtained from a MSE broadened linewidth would yield (if performed with spatial resolution) the ion-temperature profile near the wall as well as time- (if time-resolution spectroscopy was used) and spatially resolved temperature variations in the injected beam of heating neutrals.

B. Stars

It is well known that certain white dwarfs possess fields as large as 100's of kG.[32] Very large linewidths as well as "anomalous" partial continua radiation have been observed from some of these objects.[32] Although precise analysis of line shapes would be very difficult due to uncertainties in the knowledge of the appropriate velocity distributions, and the homogeneity and direction of the field, in such high magnetic fields the MSE probably plays a dominant role and cannot be ignored in spectral interpretations. In fact, if the MSE is large enough it could be the source of the observed partial continua by broadening lines into each

other. Finally, we note that a MSE broadened linewidth could be used to estimate the magnetic field at the source provided one determines (or assumes) a source temperature. Of course, largely inhomogeneous fields can also give rise to large linewidths, but the fact that Zeeman shifts of some spectral lines have been measured indicates that at least in those cases the emission emanates from fairly homogeneous field regions.

VI. CONCLUSIONS

We have analyzed the effect of the motional Stark field on the emission line shape of an atomic transition. It has been shown that the new line shape acquires a Doppler-free edge as well as a very broad tail. The Doppler-free edge has been used to determine the $7\,^1S$-$9\,^1P$ energy interval in ^{4}He with a precision better than 1 ppm. The data has also provided measurements of the Zeeman parameters of ^{4}He up to fourth order in the field B. The broad tail has been shown to be possibly important in other systems such as hot plasmas and white dwarfs. Further work on ^{4}He should provide accurate values for He quantum defects, while the application of the MSE to plasmas and white dwarfs should prove to be useful and important.

ACKNOWLEDGMENTS

We wish to thank K. B. MacAdam and D. Kleppner for useful comments regarding this work. This work was supported by the NSF.

---

*Guest scientist at the Francis Bitter National Magnet Laboratory, M. I. T., Cambridge, Mass. 02139.

[1]M. Rosenbluh, T. A. Miller, D. M. Larsen, and B. Lax, Phys. Rev. Lett. 39, 874 (1977).

[2]T. A. Miller, R. S. Freund, Adv. Magn. Reson. 9, 49 (1977), and references therein, also G. Chassanov, B. Zegarski, T. A. Miller, M. Rosenbluh, R. Panock, and B. Lax, Phys. Rev. A (to be published).

[3]K. B. MacAdam and W. H. Wing, Phys. Rev. A 15, 678 (1977) and references therein.

[4]H. J. Beyer and K. J. Kollath, J. Phys. B 10, L5 (1977), and references therein.

[5]T. N. Chang and R. T. Poe, Phys. Rev. A 14, 11 (1976), and references therein.

[6]B. Schiff, Y. Accad, and C. L. Pekeris, Phys. Rev. A 8, 2272 (1973), and references therein.

[7]C. Deutsch, Phys. Rev. A 13, 2311 (1976), and references therein.

[8]A. Temkin and A. Silver, Phys. Rev. A 10, 1439 (1974).

[9]R. F. Stebbings, Science 193, 537 (1976).

[10]T. F. Gallagher, R. M. Hill, and S. A. Edelstein, Phys. Rev. A 13, 1448 (1976).

[11]R. R. Freeman and D. Kleppner, Phys. Rev. A 14, 1614 (1976).

[12]R. Romestain, S. Geschwind, and G. E. Devlin, Phys. Rev. Lett. 39, 1583 (1977).

[13]W. C. Martin, J. Phys. Chem. Ref. Data 2, 257 (1973), and references therein.

[14]W. E. Lamb and T. H. Maiman, Phys. Rev. 105, 573 (1957).

[15]F. M. J. Pichanick, R. D. Swift, C. E. Johnson, and V. W. Hughes, Phys. Rev. 169, 55 (1968).

[16]M. Rosenbluh, Ph.D. thesis (Massachusetts Institute of Technology, 1978) (unpublished).

[17]M. J. Seaton, Proc. Phys. Soc. 88, 815 (1966).

[18]Described in M. Rosenbluh, M. S. thesis (Massachusetts Institute of Technology, 1975) (unpublished).

[19]G. Adams (private communication). The apparatus is also described in Ref. 16.

[20]K. M. Baird, H. D. Riccius, and K. J. Sensen, Opt. Commun. 6, 91 (1972).

[21]L. C. Green, N. C. Johnson, and E. K. Kolchin, Astrophys. J. 144, 369 (1966).

[22]Normally the hydrogen atom and some molecules have a linear Stark effect because their different angular momentum states are degenerate, or nearly so. Because we are considering an electric field perpendicular to the magnetic field (the z axis) the important matrix elements are $\langle u_1|x|u_2\rangle$ and thus we see that only states with $\Delta m_l = \pm 1$ are mixed. However, because we are in a magnetic field these levels can no longer be degenerate and thus the perpendicular first-order Stark effect disappears. Note that in the magnetic field direction a linear Stark effect remains since $\Delta m_l = 0$ levels are mixed and these levels remain degenerate.

[23]Reference 1 has a number of misprints including the quantity to which Eq. (4) should be compared. It should read on p. 877 as $\Delta\omega_D\,[4\gamma\,(\ln 2)^{1/2}]^{-1}$. Some other misprints are a factor of 2π missing after the second equal sign in Eq. (1) and the figure caption for Fig. 2(b) should read $R34$ rather than $R24$.

[24]These coefficients can be found in a number of places including, H. R. Griem, *Plasma Spectroscopy* (McGraw-Hill, New York, 1964), where the coefficients are listed for $n = 1$–7.

[25]In the case of the hydrogen atom or molecules with nearly degenerate states, we note that the energy denominator in Eq. (13) is entirely due to the magnetic field. Due to the symmetry of the Zeeman sublevels with respect to each other, however, the polarizability of hydrogen remains small even for large n values.

[26]A. Abragam and J. H. Van Vleck, Phys. Rev. 92, 1448 (1953).

[27]L. I. Schiff and H. Snyder, Phys. Rev. 55, 59 (1939).

[28]This is especially true for the case of helium since the quantum-defect differences of the states we are concerned with are smaller even than those for Na, for which this approximation has been shown to be reasonable in Ref. 27.

[29]E. R. Cohen and B. N. Taylor, J. Phys. Chem. Ref. Data 2, No. 4 (1973).

[30]R. Parker (private communication).

[31]J. E. Osher, in *Plasma Diagnostic Techniques*, edited by R. H. Huddlestone and S. L. Leonard (Academic, New York, 1965), p. 561.

[32]R. H. Garstang, Rep. Prog. Phys. 40, 105 (1977).

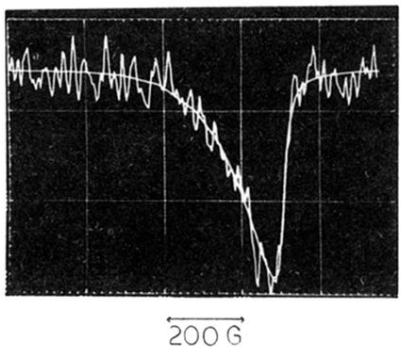

FIG. 3. Observed and calculated magnetic resonance line shape with a B_0 of 27.068 kG (on the $m_I = +1$ branch of the $9\,^1P$ state). The averaging time for obtaining the line shape was 7 min, with 5 mW/cm^2 of $R30$(10-μm branch) laser power. The excitation electron current was 1 mA and the gas pressure was 15 μm. The calculated line shape assumed a temperature of 440°K, a velocity-independent homogeneous width of 25 G and a motional Stark shift for a v_0 atom of 56 G.